$Z = 50$ core stability in ^{110}Sn from magnetic-moment and lifetime measurements

G. J. Kumbartzki,[1,*] N. Benczer-Koller,[1] K.-H. Speidel,[2] D. A. Torres,[3] J. M. Allmond,[4] P. Fallon,[5] I. Abramovic,[6] L. A. Bernstein,[5,6,7] J. E. Bevins,[6] H. L. Crawford,[5] Z. E. Guevara,[3] G. Gürdal,[8] A. M. Hurst,[5] L. Kirsch,[6] T. A. Laplace,[7,6] A. Lo,[6] E. F. Matthews,[6] I. Mayers,[6] L. W. Phair,[5] F. Ramirez,[3] S. J. Q. Robinson,[8] Y. Y. Sharon,[1] and A. Wiens[5]

[1]*Department of Physics and Astronomy, Rutgers University, New Brunswick, New Jersey 08903, USA*
[2]*Helmholtz-Institut für Strahlen- und Kernphysik, Universität Bonn, D-53115 Bonn, Germany*
[3]*Departamento de Física, Universidad Nacional de Colombia, Carrera 30 No 45-03, Bogotá D.C., Colombia*
[4]*Physics Division, Oak Ridge National Laboratory, Oak Ridge, Tennessee 37831, USA*
[5]*Nuclear Science Division, Lawrence Berkeley National Laboratory, Berkeley, California 94720, USA*
[6]*Department of Nuclear Engineering, University of California, Berkeley, California 94720, USA*
[7]*Lawrence Livermore National Laboratory, Livermore, California 94551, USA*
[8]*Physics Department, Millsaps College, Jackson, Mississippi 39210, USA*

(Received 21 December 2015; revised manuscript received 8 March 2016; published 18 April 2016)

Background: The structure of the semimagic $_{50}$Sn isotopes were previously studied via measurements of $B(E2; 2_1^+ \rightarrow 0_1^+)$ and g factors of 2_1^+ states. The values of the $B(E2; 2_1^+)$ in the isotopes below midshell at $N = 66$ show an enhancement in collectivity, contrary to predictions from shell-model calculations.
Purpose: This work presents the first measurement of the 2_1^+ and 4_1^+ states' magnetic moments in the unstable neutron-deficient ^{110}Sn. The g factors provide complementary structure information to the interpretation of the observed $B(E2)$ values.
Methods: The ^{110}Sn nuclei have been produced in inverse kinematics in an α-particle transfer reaction from ^{12}C to ^{106}Cd projectiles at 390, 400, and 410 MeV. The g factors have been measured with the transient field technique. Lifetimes have been determined from line shapes using the Doppler-shift attenuation method.
Results: The g factors of the 2_1^+ and 4_1^+ states in ^{110}Sn are $g(2_1^+) = +0.29(11)$ and $g(4_1^+) = +0.05(14)$, respectively. In addition, the $g(4_1^+) = +0.27(6)$ in ^{106}Cd has been measured for the first time. A line-shape analysis yielded $\tau(^{110}\text{Sn}; 2_1^+) = 0.81(10)$ ps and a lifetime of $\tau(^{110}\text{Sn}; 3_1^-) = 0.25(5)$ ps was calculated from the fully Doppler-shifted γ line.
Conclusions: No evidence has been found in ^{110}Sn that would require excitation of protons from the closed $Z = 50$ core.

DOI: 10.1103/PhysRevC.93.044316

I. INTRODUCTION

The tin isotopes are recognized as one of the best environments for studying nuclear structure and the shell model in the intermediately heavy nuclei. Sn is the isotope chain with the largest number of stable isotopes and potentially can be studied experimentally over the region between the unstable doubly magic ^{100}Sn ($N = 50$) and ^{132}Sn ($N = 82$) and perhaps beyond. The Sn nuclei, with $Z = 50$, are semimagic and thus exhibit a closed proton shell. In this particular case, mainly valence neutrons are expected to determine the structure of the energy levels and the transitions between them. In a simple shell-model picture, the nuclei near the doubly magic numbers of protons and neutrons should exhibit single-particle characteristics, while in midshell they should show collective aspects.

Extensive spectroscopic measurements of energy levels, lifetimes, and/or $B(E2)$ reduced transition probabilities, and electromagnetic moments, μ and Q, have been carried out in the Sn isotopic chain. The reduced transition probability data in $^{104-134}$Sn (Refs. [1–10] and references therein), follow only above midshell ($A = 116$) the parabola-like curve of the shell-model expectations [6]. For nuclei below midshell the $B(E2)$ values are larger than expected but finally decrease at $N = 54$, as the doubly closed shell $Z = N = 50$ is approached. It has been suggested that proton excitations across the $Z = 50$ shell gap have to be invoked as an explanation of the enhanced collectivity.

Magnetic moments of the 2_1^+ states were previously measured in the even-even stable $^{112-124}$Sn isotopes [9,11–13] as well as in radioactive $^{126-128}$Sn [14,15]. However, experiments using transient field (TF) or recoil-in-vacuum techniques and beam energies both below and above the Coulomb barrier yielded results which challenge comparisons with theoretical calculations.

The measurements of the magnetic moments offer a specific handle in the determinations of the nuclear structure by distinguishing between possible neutron and proton configurations. The g-factor measurement in the radioactive ^{110}Sn could shed light on the role of protons in the interpretation of the transition probabilities for the neutron-deficient Sn isotopes.

In the isotopes lighter than ^{112}Sn, the neutrons may occupy the orbitals $g_{7/2}$ and $d_{5/2}$, for which the magnetic moments should, respectively, be positive or negative. Proton excitations out of the closed core into the $g_{7/2}$ orbital would yield large positive g factors. In fact, ^{110}Sn lies between ^{109}Sn ($5/2^+_{gs}$; $g < 0$) and ^{111}Sn($7/2^+_{gs}$; $g > 0$) and a determination of even the sign of its magnetic moment would yield significant structure information.

*kum@physics.rutgers.edu

 ©2016 American Physical Society

Several theoretical approaches have focused on g factors in this region. These include, among others, the quasiparticle random-phase approximation (QRPA) [16] and the relativistic QRPA (RQRPA) [17] approach. Shell-model calculations based on the nucleon-pair approximation, as well as calculations using a low-momentum interaction and the high-precision CD-Bonn free nucleon-nucleon potential, have also been carried out [13,18–20].

While the main focus of this project is the measurement of magnetic moments, the lifetime of the $2_1{}^+$ state in ^{110}Sn has also been determined from the same data when they are analyzed via the Doppler-shift-attenuation method (DSAM). In addition, this experiment yields new data on the magnetic moment and lifetime of the $4_1{}^+$ state in Coulomb-excited ^{106}Cd beam nuclei.

II. THE EXPERIMENT

The experiment was performed at the Lawrence Berkeley National Laboratory (LBNL) 88-Inch cyclotron. The ^{110}Sn was produced via an α-particle transfer to a beam of isotopically pure ^{106}Cd ions impinging on a carbon layer at the front of a multilayer target. The specific reaction is ^{12}C (^{106}Cd, ^{8}Be) ^{110}Sn. The ^{8}Be nuclei decay spontaneously into two α particles.

The experiment and setup were similar to those described in Ref. [21]. The components of the multilayer target for this experiment are shown in Table I.

Beam energies of 390, 400, and 410 MeV were employed to find the best α-transfer yield. The bulk of the data was taken at 410 MeV. At this energy the beam has lost about 20 MeV when reaching the middle of the carbon layer and its energy there is close to that of the Coulomb barrier. As found in Ref. [21], the α-transfer reaction is optimal near the Coulomb barrier between the projectile and carbon. The newly created ^{110}Sn and Coulomb-excited ^{106}Cd recoils traverse the gadolinium layer where they experience the TF. These nuclei are stopped in the copper backing. Their decay γ rays are detected in coincidence with forward-scattered particles.

The target was mounted between the pole tips (8-mm gap) of a liquid-nitrogen-cooled magnet. The gadolinium layer of the target was magnetized by a field of 0.07 T. Its direction was reversed every 150 s during the measurements. The particle detector was a 300-mm^2 Si surface-barrier detector (Canberra PIPS). The detector was placed 25 mm downstream of the target at 0° to the beam direction. Its opening angle was ±20°. The detector was covered by a 5.6 mg/cm^2 thick copper foil, which stopped the noninteracting beam particles passing through the target but was transparent to the light particles resulting from the reactions. The different particle groups were well separated in the 300-μm-thick detector as is shown in Fig. 1.

TABLE I. Composition of multilayer target. All thicknesses are in mg/cm^2.

C	Gd	Ta	Cu
0.636	8.34	1.1	5.40

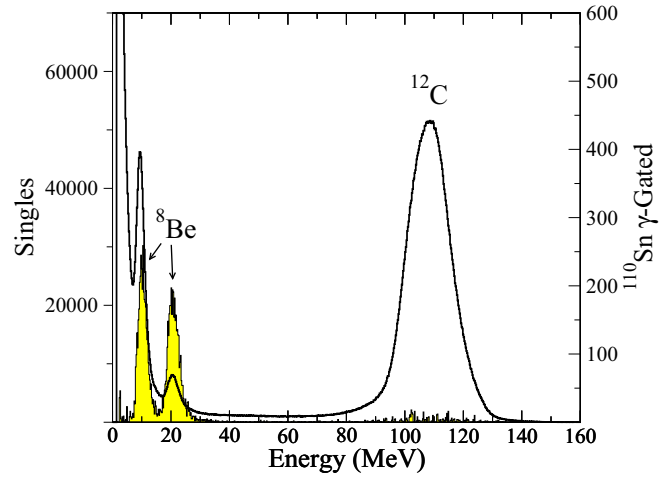

FIG. 1. Single-particle spectrum observed in the Si detector. Also shown are particles in coincidence with gates set on time and γ rays corresponding to ^{110}Sn. The two peaks labeled ^{8}Be relate to the detection of only one or both α particles (2α) from the ^{8}Be breakup.

The γ rays were recorded in four clover HPGe detectors from the ORNL and LBNL inventories. These were located 125 mm away from the target at angles of $\theta = \pm 60°$ and $\pm 120°$ with respect to the beam direction. At that distance the individual elements of the clover detectors subtend angles of $\pm 8°$ with respect to the center of the clover enclosure.

The preamplifier output signals of all detectors were digitized using a PIXIE-4 system [22]. Their time stamps and energies were written to disk. The data handling and analysis were performed as described in greater detail in Ref [21].

Typical particle-γ coincidence spectra gated on the ^{12}C and the 2α peaks, displaying respectively the decay of the excited energy levels of ^{106}Cd and ^{110}Sn, are shown in Fig. 2. For ^{110}Sn only three prominent γ lines are seen in the spectrum referring to the ($2_1{}^+ \rightarrow 0_1{}^+$) 1212 keV, the ($4_1{}^+ \rightarrow 2_1{}^+$) 985 keV, and the ($6_1{}^+ \rightarrow 4_1{}^+$) 280 keV transitions. This picture clearly

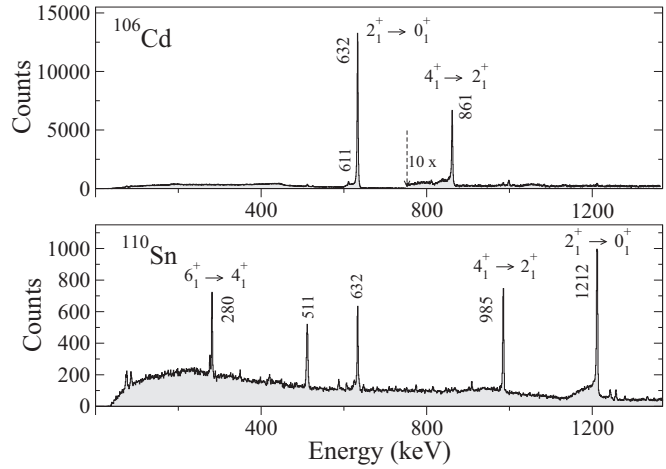

FIG. 2. Coincidence γ spectra. The ^{106}Cd spectrum was gated on the ^{12}C peak in Fig. 1 while the ^{110}Sn spectrum was gated on the 2α peak of the ^{8}Be breakup.

TABLE II. The kinematic information related to the transient field measurement at 410 MeV. $\langle E\rangle_{\rm in}$, $\langle E\rangle_{\rm out}$, $\langle v/v_0\rangle_{\rm in}$, and $\langle v/v_0\rangle_{\rm out}$ are the energies, in MeV, and velocities of the excited probe ions as they enter into, and exit from, the gadolinium layer; $v_0 = e^2/\hbar$ is the Bohr velocity. $T_{\rm eff}$ is the effective time the transient field acts on the ions traversing the ferromagnetic layer.

Nucleus	$\langle E\rangle_{\rm in}$	$\langle E\rangle_{\rm out}$	$\langle \frac{v}{v_0}\rangle_{\rm in}$	$\langle \frac{v}{v_0}\rangle_{\rm out}$	$T_{\rm eff}$ (fs)
^{106}Cd	232	46	9.4	4.2	715
^{110}Sn	252	54	9.6	4.5	438

demonstrates the direct and highly selective nature of the α-transfer reaction in contrast to a fusion reaction. In the Coulomb excitation of ^{106}Cd mainly the $2_1{}^+$ and the $4_1{}^+$ states are seen via their $E2$ transitions in the spectrum.

A. Precession measurement

The magnetic properties of the ^{106}Cd and the ^{110}Sn nuclei were measured simultaneously. The g factor of the $2_1{}^+$ state in ^{106}Cd was measured previously [23]. Its value is used as a check on the experiment and also serves to calibrate the transient field strength.

In a TF measurement the spin precession of the aligned nuclei as they pass through the magnetized ferromagnetic layer causes a rotation of the angular distribution of the decay γ radiation. The precession angle is derived from counting rate changes in the stationary γ detectors when the polarizing field, which is perpendicular to the detection plane of the γ detectors, is reversed. The so-called rate effect ϵ, as described in many publications (e.g., Ref. [24]), is calculated from peak intensities in the spectra of four γ detectors. Together with the logarithmic slope, $S(\theta_\gamma) = [1/W(\theta_\gamma)]dW/d\theta_\gamma$ of the angular correlation relevant for the precession, the precession angle

$$\Delta\theta = \frac{\epsilon}{S(\theta_\gamma)} = g\frac{\mu_N}{\hbar}\int_{t_{\rm in}}^{t_{\rm out}} B_{\rm TF}[v(t), Z]e^{-t/\tau}dt$$

is obtained. In this expression g is the g factor of the excited state, μ_N is the nuclear magneton, and $B_{\rm TF}$ is the effective transient field acting on the nucleus during the time interval $(t_{\rm out} - t_{\rm in})$ spent by the ions in the gadolinium layer. The exponential factor accounts for the nuclear decay during the transit time of the ions through the gadolinium layer. The relevant kinematic information for the transient-field calculation is summarized in Table II.

B. Angular correlations

The angular correlations for the states in both ^{106}Cd and ^{110}Sn were also derived from the precession data. The peak intensities of the $2_1{}^+ \rightarrow 0_1{}^+$ and $4_1{}^+ \rightarrow 2_1{}^+$ transitions in the spectra of each clover crystal, summed over both field directions and corrected for relative efficiencies, are plotted in Fig. 3. The relative efficiencies were measured with a ^{152}Eu source in the target position before and verified immediately after the experiment using the activity of the target. The solid lines represent fits to the angular correlation function restrained

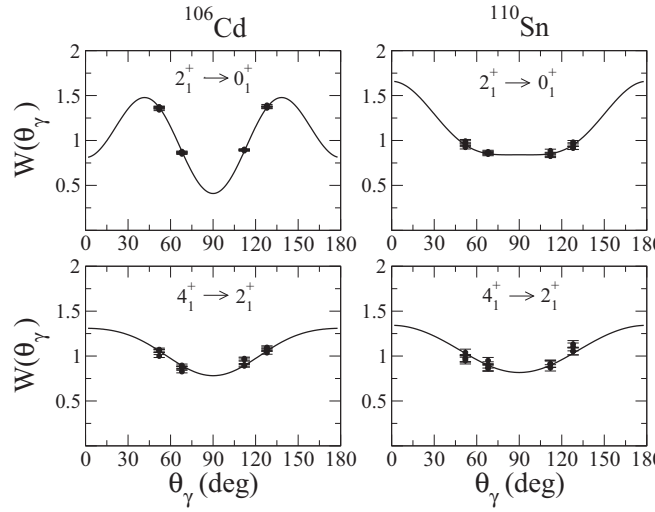

FIG. 3. Angular particle-γ correlations measured at a beam energy of 410 MeV.

to only physical parameters for the correlation coefficients

$$W(\theta_\gamma) = 1 + A_2Q_2P_2(\cos\theta_\gamma) + A_4Q_4P_4(\cos\theta_\gamma).$$

Here the $P_k(\cos\theta_\gamma)$ are the Legendre polynomials, the A_k are the experimental angular-correlation coefficients, which depend on the multipolarity of the γ-ray transition, and the Q_k are attenuation coefficients accounting for the finite solid angle of the γ detectors.

C. Lifetimes

Because of the high recoil velocities of the ions, the lines of the short-lifetime transitions exhibit prominent lineshapes (Fig. 2) suitable for lifetime analysis using the DSAM technique. The LINESHAPE [25] code was used. The Doppler-broadened shape of the γ lines was fitted to the reaction kinematics by applying stopping powers [26] to Monte Carlo simulations and including second-order Doppler effects as well as the finite size and energy resolution of the γ detectors. A sample fit for the 1212-keV line in ^{110}Sn is shown in Fig. 4. The short-lived $2_1{}^+$ state is fed about 40% from the long-lived $6_1{}^+$ and $4_1{}^+$ states, which accounts for nearly all of the stopped components in the lineshape. Also excited in ^{110}Sn is a $3_1{}^-$ state at 2458.4 keV which decays into the $2_1{}^+$, contributing about 8% to its intensity. The lifetime of the $3_1{}^-$ state was unknown, but from the fully Doppler-shifted peak positions at 52° and 68°, together with the reaction kinematics and energy loss in the multilayer target, a lifetime of 0.25(5) ps was derived. Unfortunately, this $3_1{}^- \rightarrow 2_1{}^+$ fully shifted and Doppler-broadened γ transition of 1246.4 keV also falls under the lineshape of the 1212-keV line at backward angles. By including various scenarios for the feeding contributions and using the detectors at different angles, a number of fits produced lifetimes close to the literature value calculated from $B(E2)$ measurements. Overall, in this work, the lineshape fits give an average $\tau(^{110}\text{Sn}; 2_1{}^+) = 0.81(10)$ ps, which is slightly larger than the NNDC value of 0.69(6) ps [27].

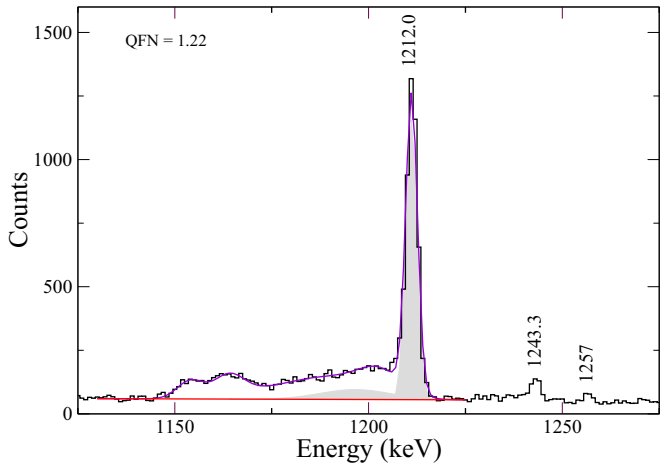

FIG. 4. LINESHAPE fit of the $2_1^+ \rightarrow 0_1^+$ γ line in ^{110}Sn as observed in two clover segments at 128°. The greyed-out areas represent feeding intensities. QFN represents the normalized χ^2.

D. Magnetic moments

The Coulomb excitation of the 2_1^+ state in ^{106}Cd provided a solid check of the precession measurement. At a beam energy of 400 MeV, for which feeding is the lowest, the known g-factor value was reproduced. In later runs with various beam intensities, the Cd value was taken to monitor and determine the magnetization (temperature) of the target spot. Indeed, a strong correlation between the beam current, represented by the measured single-particle rate, and the precession effect of the $2_1^+ \rightarrow 0_1^+$ transition in ^{106}Cd was observed.

The results are summarized in Table III. The g factor of the 2_1^+ of ^{110}Sn was analyzed from γ spectra in coincidence with the 2α-peak (Fig. 1). Because of considerable feeding by the long-lived states in the $6_1^+ \rightarrow 4_1^+ \rightarrow 2_1^+$ cascade, and to avoid feeding corrections, only the Doppler-shifted part of the 1212-keV γ line was used in the precession analysis. This procedure reduces the counting statistics but avoids even larger errors caused by the error propagation in the feeding corrections [31]. The very short lifetime of the state affects the effective transit time in the gadolinium layer of the target and the g factor. The slightly shorter literature lifetime of 0.69 ps would increase the value of the g factor quoted in Table III by 7%. The g factors of the 4_1^+ and 6_1^+ states were determined from γ spectra gated on both α peaks in Fig. 1. Both values are within the errors close to zero. For the 4_1^+ state a lifetime of 4 ps was used, which is long enough to not affect the quoted g factor.

The g factor of the 4_1^+ state in ^{106}Cd was measured for the first time. The state has a short lifetime and is fed by a second 4^+. The literature value [29] is $\tau(^{106}\text{Cd}; 4_1^+) = 1.26(15)$ ps. A lineshape analysis of the current data favors a longer lifetime of $\tau = 2.5(2)$ ps. The longer lifetime would reduce the g-factor value quoted in Table III by ∼25%. More details of the ^{106}Cd results will be presented in a forthcoming paper.

III. DISCUSSION AND THEORY

None of the theoretical approaches shown in Fig. 5 can describe the $g(2_1^+)$ factors of *all* the Sn isotopes. Although, the common trend from positive to negative g-factor values is reproduced. No shell-model calculation explicitly breaking the $Z = 50$ shell was published.

The results of Ansari and Ring [17] agree with the measured $g(2_1^+)$ of the present paper but not with most of the measured values for other Sn isotopes. The other two calculations in Fig. 5 are within 1.7 standard deviations but lower than the measured value.

Jiang *et al.* [19] calculated the magnetic moments of the first 2^+ states in the Sn isotopes within the framework of the nucleon-pair approximation of the shell model. Their calculation yields a g factor for ^{110}Sn about three times smaller than the measured value. Furthermore, the authors used an effective $g_{\nu l} = +0.09$, rather than the generally accepted value, $g_{\nu l} = -0.1$ [32]. This sign inversion could alter considerably the final result.

TABLE III. Experimental results for states in ^{110}Sn and ^{106}Cd. Also included are the slopes for full clovers and precession angles. $\Delta\theta$ ($g = 1$) was calculated using the Rutgers parametrization [28]. The lifetimes are taken from the National Nuclear Data Center (NNDC) database [27,29].

	E_{Beam}	I_i^π	E_γ	τ	$\Delta\theta$ ($g = 1$)	$\lvert S(60°)\rvert$	$\Delta\theta$	g	
	(MeV)		(keV)	(ps)	(mrad)	(mrad $^{-1}$)	(mrad)	This work	Others
^{110}Sn									
	410	2_1^+	1212.0	0.81(10)[a]	65.8	0.384(37)	18.8(68)	+0.29(11)	
		4_1^+	984.0	>4.0[b]	92.6	0.463(55)	4.7(130)	+0.05(14)	
		6_1^+	280.2	$8.1(4)\cdot10^3$	103.0	0.565(120)	0.8(191)	+0.01(19)	+0.012(3)[c]
^{106}Cd									
	400	2_1^+	632.7	10.49(12)	98.5	1.76(3)[d]	39.14(94)	+0.398(22)	+0.393(31)[e]
	410	4_1^+	861.2	1.26(16)	73.5	0.66(3)	19.6(40)	+0.27(6)	

[a]This work. The NNDC value is $\tau(2_1^+) = 0.69(6)$ ps [27].
[b]The lifetime is unknown. The adopted value agrees with systematics in neighboring isotopes. The lineshape shows no discernible Doppler-shifted component.
[c]Reference [30].
[d]$|S(67°)|$
[e]Reference [23].

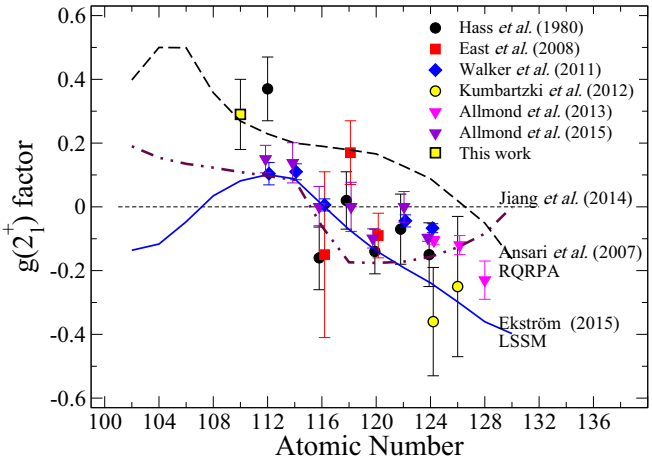

FIG. 5. Compilation of experimental $g(2_1{}^+)$ factors from Refs. [9,11–15]. The LSSM calculation is based on the ^{100}Sn core calculation of Ref. [6] as published in Ref. [13] and extended by Ekström [33] to the neutron-deficient Sn isotopes.

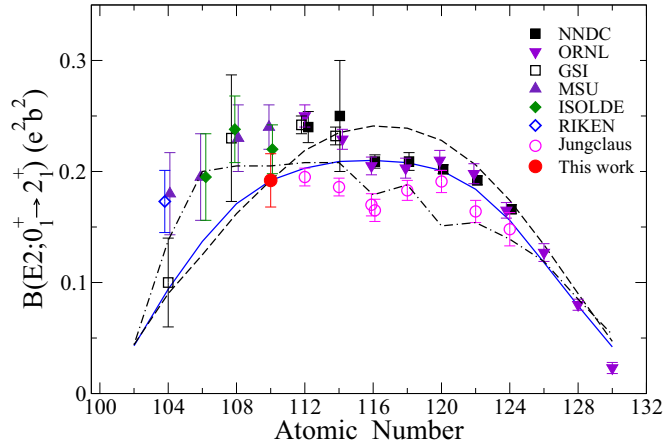

FIG. 6. Compilation of measured $B(E2; 0^+_{gs} \rightarrow 2_1{}^+)$ values of the even tin isotopes. The majority of the data [1,2,4–6,8,9,36] are from Coulomb-excitation cross-sectional measurements. The Jungclaus data [10] and this work (circles) are from DSAM lifetime measurements. The solid and dashed curves show shell-model calculations from Ref. [6] using a ^{100}Sn and ^{90}Zr closed core, respectively. Also shown are calculations using the quasiparticle phonon model from Ref. [37].

The shell-model calculation by Ekström [33] based on a stable ^{100}Sn core as described in Ref. [13] also underpredicts the present ^{110}Sn result. This calculation predicts a downturn of the g factors for the proton-rich isotopes and overall agrees best with the experimental data.

In the present work, large-scale shell model (LSSM) calculations were carried out for ^{110}Sn adopting the SN100PN interaction [34]. A ^{100}Sn core was employed and proton excitations were excluded. The neutron orbital space included $g_{7/2}$, $d_{5/2}$, $d_{3/2}$, and $s_{1/2}$ with and without $h_{11/2}$. The best agreement with the experimental data was obtained without the $h_{11/2}$ orbital, $g_{\nu l} = +0.1$ and $g_{\nu s} = 0.75 g_s^{\rm free}$, values similar to those used in Ref. [19]. The resulting g factors were $g(2^+) = +0.15$, $g(4^+) = +0.12$, and $g(6^+) = +0.1$. With $g_{\nu l} = -0.1$, all three g factors turn negative. Furthermore, the inclusion of the $h_{11/2}$ orbital considerably reduced these results.

If the wave functions of the states of interest in ^{110}Sn were of purely neutron nature, in the spirit of the seniority scheme, at a minimum two neutrons not coupled to zero are required in the available $(g_{7/2})$ and $(d_{5/2})$ orbitals near the Fermi level to form excited states.

Therefore, in a simple single-particle approach, the case of two neutrons in the $(g_{7/2})^2$ and the mixed $[(g_{7/2})^1,(d_{5/2})^1]$ configurations is considered. The expression

$$g_j = g_l \pm \frac{(g_s - g_l)}{(2l+1)} \quad \text{with} \quad j = l \pm 1/2$$

gives $g^{\rm cal}(g_{7/2}) = +0.208$ and $g^{\rm cal}(d_{5/2}) = -0.654$ using effective values for the neutron spin and orbital g factors, $g_s^{\rm eff} = -3.826 \times 0.75$ and $g_l^{\rm eff} = -0.1$. Thus the configuration $(g_{7/2})^2$ yields $g(2_1{}^+) = g(4_1{}^+) = g(6_1{}^+) = +0.208$. Then, the expression [35]

$$g(j_1 \otimes j_2, I) = \frac{(g_1+g_2)}{2} + \frac{(g_1-g_2)}{2} \frac{j_1(j_1+1) - j_2(j_2+1)}{I(I+1)},$$

where $j_1 = 7/2$, $j_2 = 5/2$, and I, the total angular momentum, yields the effective g factors for the mixed configuration

$$g^{\rm cal}(2_1{}^+) = +0.28, \quad g^{\rm cal}(4_1{}^+) = -0.07, \quad g^{\rm cal}(6_1{}^+) = -0.151.$$

The results from the two configurations, when averaged, yield values of

$$g^{\rm cal}(2_1{}^+) = +0.24, \quad g^{\rm cal}(4_1{}^+) = +0.07, \quad g^{\rm cal}(6_1{}^+) = +0.03.$$

These values are in very good agreement with the observed g factors of the present work (Table III). Any inclusion of the $(d_{5/2})^2$ configuration leads to smaller or negative g factors in contrast to the experimental results. In this context it is noteworthy to mention that any contribution from protons excited from the core would significantly increase these values due to the corresponding large positive g values of the relevant proton orbitals.

The $B(E2)$ value deduced from the present lifetime value of the $2_1{}^+$ state:

$$B(E2; 0_1{}^+ \rightarrow 2_1{}^+)^{\rm exp} = 0.192(24) e^2{\rm b}^2.$$

agrees with shell model calculations based on the doubly magic ^{100}Sn core and ^{90}Zr core [6] (see Fig. 6). The result is slightly lower than the two previous Coulomb-cross-section-based values of 0.220(22) e^2b^2 [5] and 0.240(20) e^2b^2 [4].

The $g(2_1{}^+)$ factor is positive but not large enough to require proton excitation from the $Z = 50$ core, an observation additionally supported by the small g factors for the $4_1{}^+$ and $6_1{}^+$ states.

This conclusion is also supported by a very recent lifetime measurement of the $2_1{}^+$ state of the isotonic ^{112}Te isotope [38]. This nucleus has the same neutron number as ^{110}Sn, $N = 60$, with two additional protons outside the magic proton core. In spite of an expected polarizing effect of the two valence

protons on the proton core, the deduced $B(E2)$ value is well explained by shell model calculations based on a ^{100}Sn core. The authors also expect this robustness of the $Z = 50$ core for all ^{52}Te isotopes.

IV. SUMMARY

The current work presents the first measurements of the $g(2_1{}^+)$ and $g(4_1{}^+)$ factors in the unstable neutron-deficient even Sn isotopes. Altogether, the present data are in agreement with the classical seniority scheme of the shell model. These data can be understood without proton excitation from the $Z = 50$ core. In view of several $B(E2)$ measurements on light neutron-deficient Sn isotopes claiming proton core excitations and in view of the present observations and results, further measurements of magnetic moments and lifetimes for other neutron-deficient Sn isotopes with radioactive Sn ion beams are highly desirable.

ACKNOWLEDGMENTS

The authors thank the Berkeley 88-Inch Cyclotron staff for their help in setting up the experiment and providing the cadmium beam. The target was prepared by P. Maier-Komor at the Technische Universität Munich, Germany. The authors are grateful to L. Zamick for many discussions and suggestions about the theoretical interpretation of the g factor results. K.-H.S. acknowledges support by the Deutsche Forschungsgemeinschaft under Grant No. SP190/18-1. D.A.T., Z.E.G., and F.R. acknowledge support by Colciencias under Contract No. 110165842984-2015. Y.Y.S. acknowledges support from Stockton University under a Research and Professional Development award. The work has been supported in part by the US National Science Foundation and by the US Department of Energy under Contracts No. DE-AC02-05CH11231 and No. DE-AC52-07NA27344.

[1] P. Doornenbal, S. Takeuchi, N. Aoi, M. Matsushita, A. Obertelli, D. Steppenbeck, H. Wang, L. Audirac, H. Baba, P. Bednarczyk *et al.*, Phys. Rev. C **90**, 061302 (2014).
[2] J. M. Allmond, D. C. Radford, C. Baktash, J. C. Batchelder, A. Galindo-Uribarri, C. J. Gross, P. A. Hausladen, K. Lagergren, Y. Larochelle, E. Padilla-Rodal *et al.*, Phys. Rev. C **84**, 061303 (2011).
[3] A. Ekström, J. Cederkäll, C. Fahlander, M. Hjorth-Jensen, F. Ames, P. A. Butler, T. Davinson, J. Eberth, F. Fincke, A. Görgen *et al.*, Phys. Rev. Lett. **101**, 012502 (2008).
[4] C. Vaman, C. Andreoiu, D. Bazin, A. Becerril, B. A. Brown, C. M. Campbell, A. Chester, J. M. Cook, D. C. Dinca, A. Gade *et al.*, Phys. Rev. Lett. **99**, 162501 (2007).
[5] J. Cederkäll, A. Ekström, C. Fahlander, A. M. Hurst, M. Hjorth-Jensen, F. Ames, A. Banu, P. A. Butler, T. Davinson, U. D. Pramanik *et al.*, Phys. Rev. Lett. **98**, 172501 (2007).
[6] A. Banu, J. Gerl, C. Fahlander, M. Górska, H. Grawe, T. R. Saito, H.-J. Wollersheim, E. Caurier, T. Engeland, A. Gniady *et al.*, Phys. Rev. C **72**, 061305 (2005).
[7] G. Guastalla, D. D. DiJulio, M. Górska, J. Cederkäll, P. Boutachkov, P. Golubev, S. Pietri, H. Grawe, F. Nowacki, K. Sieja *et al.*, Phys. Rev. Lett. **110**, 172501 (2013).
[8] V. M. Bader, A. Gade, D. Weisshaar, B. A. Brown, T. Baugher, D. Bazin, J. S. Berryman, A. Ekström, M. Hjorth-Jensen, S. R. Stroberg *et al.*, Phys. Rev. C **88**, 051301 (2013).
[9] J. M. Allmond, A. E. Stuchbery, A. Galindo-Uribarri, E. Padilla-Rodal, D. C. Radford, J. C. Batchelder, C. R. Bingham, M. E. Howard, J. F. Liang, B. Manning *et al.*, Phys. Rev. C **92**, 041303 (2015).
[10] A. Jungclaus, J. A. Walker, J. Leske, K.-H. Speidel, A. E. Stuchbery, M. East, P. Boutachkov, J. Cederkäll, P. Doornenbal, J. L. Egido *et al.*, Phys. Lett. B **695**, 110 (2011).
[11] M. Hass, C. Broude, Y. Niv, and A. Zemel, Phys. Rev. C **22**, 97 (1980).
[12] M. East, A. Stuchbery, A. Wilson, P. Davidson, T. Kibédi, and A. Levon, Phys. Lett. B **665**, 147 (2008).
[13] J. Walker, A. Jungclaus, J. Leske, K.-H. Speidel, A. Ekström, P. Boutachkov, J. Cederkäll, P. Doornenbal, J. Gerl, R. Gernhäuser *et al.*, Phys. Rev. C **84**, 014319 (2011).
[14] G. J. Kumbartzki, N. Benczer-Koller, D. A. Torres, B. Manning, P. D. O'Malley, Y. Y. Sharon, L. Zamick, C. J. Gross, D. C. Radford, S. J. Q. Robinson *et al.*, Phys. Rev. C **86**, 034319 (2012).
[15] J. M. Allmond, A. E. Stuchbery, D. C. Radford, A. Galindo-Uribarri, N. J. Stone, C. Baktash, J. C. Batchelder, C. R. Bingham, M. Danchev, C. J. Gross *et al.*, Phys. Rev. C **87**, 054325 (2013).
[16] J. Terasaki, J. Engel, W. Nazarewicz, and M. Stoitsov, Phys. Rev. C **66**, 054313 (2002).
[17] A. Ansari and P. Ring, Phys. Lett. B **649**, 128 (2007).
[18] L. Y. Jia, H. Zhang, and Y. M. Zhao, Phys. Rev. C **75**, 034307 (2007).
[19] H. Jiang, Y. Lei, C. Qi, R. Liotta, R. Wyss, and Y. M. Zhao, Phys. Rev. C **89**, 014320 (2014).
[20] L. Coraggio, A. Covello, A. Gargano, N. Itaco, and T. T. S. Kuo, Phys. Rev. C **91**, 041301 (2015).
[21] G. J. Kumbartzki, N. Benczer-Koller, S. Burcher, A. Ratkiewicz, S. L. Rice, Y. Y. Sharon, L. Zamick, K.-H. Speidel, D. A. Torres, K. Sieja *et al.*, Phys. Rev. C **89**, 064305 (2014).
[22] X-ray Instrumentation Associates [http://www.xia.com/].
[23] S. K. Chamoli, A. E. Stuchbery, S. Frauendorfer, J. Sun, Y. Gu, R. F. Leslie, T. P. Moore, A. Wahlke, M. C. East, T. Kibédi *et al.*, Phys. Rev. C **83**, 054318 (2011).
[24] N. Benczer-Koller and G. J. Kumbartzki, J. Phys. G: Nucl. Part. Phys. **34**, R321 (2007).
[25] J. C. Wells and N. R. Johnson, Computer code LINESHAPE (1999), PD-LNL version.
[26] F. J. Ziegler, J. Biersack, and U. Littmark, *The Stopping and Range of Ions in Solids*, Vol. 1 (Pergamon, Oxford, 1985).
[27] G. Gürdal and F. G. Kondev, Nucl. Data Sheets **113**, 1315 (2012) [ENDSF: http://www.nndc.bnl.gov/nndc/ensdf/].
[28] N. K. B. Shu, D. Melnik, J. M. Brennan, W. Semmler, and N. Benczer-Koller, Phys. Rev. C **21**, 1828 (1980).

[29] D. D. Frenne and A. Negret, Nucl. Data Sheets **109**, 943 (2008) [ENDSF: http://www.nndc.bnl.gov/nndc/ensdf/].
[30] D. A. Volkov, B. I. Gorbachev, A. I. Kovalenko, A. I. Levon, O. F. Nemets, O. V. Sevastyuk, and A. A. Shevchuk, Izv. Akad. Nauk SSSR Ser. Fiz. **53**, 2188 (1989); Bull. Acad. Sci. USSR, Phys. Ser. **53**, 133 (1989).
[31] D. A. Torres, G. J. Kumbartzki, Y. Y. Sharon, L. Zamick, B. Manning, N. Benczer-Koller, G. Gürdal, K.-H. Speidel, M. Hjorth-Jensen, P. Maier-Komor *et al.*, Phys. Rev. C **84**, 044327 (2011).
[32] A. Poves, J. Sanchez-Solano, E. Caurier, and F. Nowacki, Nucl. Phys. A **694**, 157 (2001).
[33] A. Ekström (private communication).
[34] B. A. Brown, N. J. Stone, J. R. Stone, I. S. Towner, and M. Hjorth-Jensen, Phys. Rev. C **71**, 044317 (2005).
[35] A. de Shalit and I. Talmi, *Nuclear Shell Theory* (Academic Press, New York, 1963).
[36] S. Raman, C. W. N. Jr., and P. Tikkanen, At. Data Nucl. Data Tables **78**, 1 (2001).
[37] N. L. Iudice, C. Stoyanov, and D. Tarpanov, Phys. Rev. C **84**, 044314 (2011).
[38] M. Doncel, T. Bäck, D. M. Cullen, D. Hodge, C. Qi, B. Cederwall, M. J. Taylor, M. Proctor, K. Auranen, T. Grahn *et al.*, Phys. Rev. C **91**, 061304 (2015).